N72 30399

NASA CR-112116

DESIGN, FABRICATION AND CALIBRATION OF ALPHA PARTICLE DENSITOMETERS FOR MEASURING PLANETARY ATMOSPHERIC DENSITY

FINAL REPORT

Prepared by

Bach Sellers
Jean Luc Hunerwadel
Frederick A. Hanser

for

NASA Langley Research Center
Langley Station, Hampton, Virginia

Contract No.
NAS 1-9731

May 1972

PANAMETRICS, INC.
221 Crescent Street
Waltham, Massachusetts 02154

NASA CR- 112116

DESIGN, FABRICATION AND CALIBRATION OF ALPHA PARTICLE DENSITOMETERS FOR MEASURING PLANETARY ATMOSPHERIC DENSITY

FINAL REPORT

Prepared by

Bach Sellers
Jean Luc Hunerwadel
Frederick A. Hanser

for

NASA Langley Research Center
Langley Station, Hampton, Virginia

Contract No.
NAS 1-9731

May 1972

PANAMETRICS, INC.
221 Crescent Street
Waltham, Massachusetts 02154

FOREWORD

The research reported herein was carried out for the NASA Langley Research Center in Hampton, Virginia. Special appreciation is given to Mr. Gary W. Grew, the Technical Representative for the NASA Langley Research Center, for his technical guidance during the course of this effort.

This is a final report and summarizes work performed over the period January 1970 to May 1972.

ABSTRACT

An alpha particle densitometer has been developed for possible application to measurement of the atmospheric density-altitude profile on Martian entry. The device uses an Am-241 radioactive-foil source, which emits a distributed energy spectrum, located about 25-75 cm from a semiconductor detector. System response - defined as the number of alphas per second reaching the detector with energy above a fixed threshold - is given for Ar and CO_2. The altitude profile of density measurement accuracy is given for a pure CO_2 atmosphere with 5 mb surface pressure.

The entire unit, including dc-dc converters, requires less than 350 milliwatts of power from +28 volts, weighs about 0.85 lb and occupies less than 15 cubic inches volume. System accuracy is optimum in the 10^{-4} to 10^{-6} g/cm^3 range, which corresponds to 20-50 km in the Earth's atmosphere. Because of its one or two second time response, this device would, therefore, provide the basis for a highly accurate, low power, rocket borne atmospheric density probe. Alternatively, without the radioactive source it would provide the ideal basis for a simple, very low power, particle spectrometer for planetary missions.

TABLE OF CONTENTS

LIST OF ILLUSTRATIONS

LIST OF TABLES

1. INTRODUCTION

In the next few years it is expected that lander vehicles will explore the atmosphere and surface of the planet Mars. These landers will send back much scientifically important data, including the vertical atmospheric density profile, and the diurnal and seasonal surface atmospheric density variations. The vertical density profile will be measured during the entry descent, while the surface density variations will be measured during the remainder of the lander's lifetime.

Atmospheric gas density can be measured by two principal methods. The first involves measuring the gas temperature, pressure and average molecular weight, from which the gas density can be obtained through use of the gas laws. If the acceleration of gravity at the Martian surface is known as well as its variation with altitude, and if the average molecular weight of the atmosphere is known, then the vertical density profile can be obtained from pressure vs. temperature data, or from temperature or pressure vs. altitude data, provided at least one complete density measurement is made. Diurnal and seasonal variations require both pressure and temperature measurements, as well as knowledge of the average molecular weight. Since a complete density measurement requires at least one set of pressure and temperature measurements, in addition to molecular weight data, the failure of any one of these systems will preclude obtaining any absolute density measurements.

The second principal method of density measurement is a system which responds primarily to gas density. Since the interaction of nuclear and atomic radiation is generally dependent only on the amount of matter rather than its pressure and temperature, such radiation-based systems are ideally suited for direct measurement of gas density. Use of a direct density measurement along with pressure, temperature and average molecular weight measurements forms a redundant system which allows internal checks on system performance. Also, if one component fails a complete set of data is still obtained.

Of the radiation methods for density measurement the one that is the subject of this report is the α particle system. Here, as shown in Fig. 1.1, an α source is located at a fixed separation from a detector, and the variation of gas density in this space produces a change in the system response R. Two techniques can be distinguished: the first uses a "thin", or nearly monoenergetic, source, and the second uses a "thick", or distributed energy, source. For the "thin source" method R is the average energy lost; for the "thick source" method R is the count rate of all particles reaching the detector with energy above a fixed threshold.

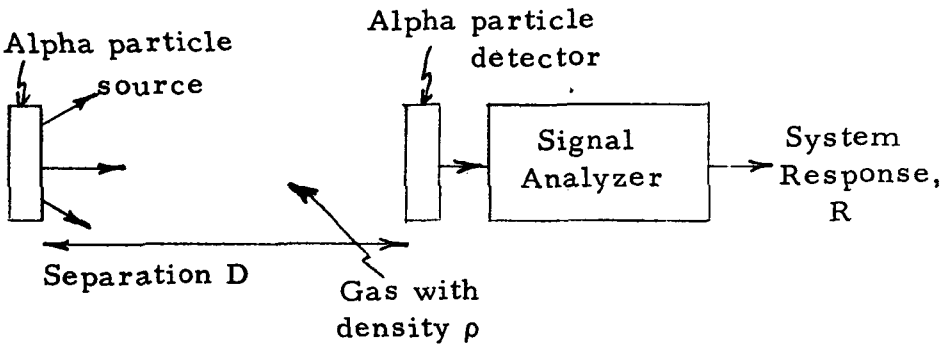

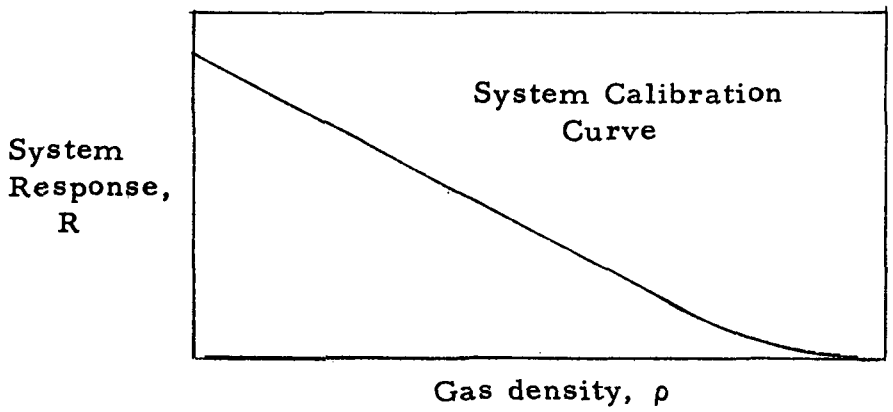

Measured density error:

$$\delta\rho = \frac{d\rho}{dR} \delta R$$

Figure 1.1 Outline of the Basic Operation of a Gas Density Measuring System Using Alpha Particles.

Both systems can be calibrated for response vs. gas density, and then used to measure absolute gas density.

An extensive study of these two alpha attenuation methods has been completed (Ref. 1.1), and as a result it was recommended that both feasibility and flight prototype models of a "thick source" system be fabricated. That work is the subject of the present report.

At the time of the previous study considerable uncertainty still existed in both the atmospheric composition and surface pressure of Mars. Hence the system response for a wide range of possible constituents was measured, including CO_2, N_2 and Ar. The response for CO_2 and N_2 was found to be very nearly the same, while that for Ar deviated in the theoretically predicted manner. Subsequently, it has been determined that the atmosphere is almost entirely CO_2 and that the surface pressure is very near 5 mb (Refs. 1.2, 1.3). As a consequence, although calibration results for the prototype are given for both CO_2 and Ar, estimates of the accuracy have been based on the response in CO_2.

In the following sections the design and fabrication of the feasibility and prototype models are presented separately, and final density accuracy and system specifications are given for the prototype unit. This entire unit, including dc-dc converters, weighs about 0.85 lb, occupies less than 15 in.^{3} and requires less than 350 milliwatts of power from the main +28 volt satellite power supply.

2. FEASIBILITY MODEL

2.1 Design Considerations

2.1.1 General

The principal purpose of the feasibility model was to demonstrate that a gas density measurement system could be designed to meet the requirements of a flight system incorporated on a Mars lander vehicle. During the design phase of the feasibility model, particular attention was therefore given to the overall power consumption of the system and the reliability of individual components.

Although overall weight and size of the feasibility model itself was of secondary importance, all components were selected to minimize physical size and weight of the final flight prototype. Design goals for the prototype were 170 mw, not including DC/DC converters, a weight of 1 lb and a volume of 13 in.^{3}. Since the digital section of the electronics employs a 14 bit counter and logic circuitry, it was advisable to choose ultra low power COS/MOS (Complementary Metal Oxide Semiconductor) integrated circuits. In addition to low quiescent power consumption, the supply voltage of these circuits covers the range from 6 to 15 volts. Thus, close regulation is obviously not required, and a simple zener referenced series regulator can be used as the supply. Some question existed with regard to the potential for radiation damage to these very low power components, and the results of an investigation of this problem are given below.

For the analog section hybrid amplifier modules were chosen because of their low power and small size. These hybrid microcircuits have been specifically developed for space applications by Solid State Radiations, Incorporated. Amplifiers of this type were previously flown on several rockets and on satellites with no failures occurring. Because of the low power consumption (about 50 mw) of the analog section a DC/DC converter would be very inefficient. A series regulator was chosen for this supply to conserve power and space.

2.1.2 Radiation Damage to COS-MOS Components

The two major sources of radiation damage for equipment launched from earth to Mars are first, the radiation of the Van Allen belts, which must be crossed shortly after launch, and second, solar flare protons. In this analysis it is assumed that the components are shielded from the radiation by the satellite itself with the equivalent

of about 1 g/cm^2 of material, so that only electrons greater than 1.5 MeV, and protons greater than 30 MeV, need be considered.

1) Van Allen Belt Radiation - The general characteristics of the earth's trapped radiation belts are summarized in Ref. 2.1 (4 volumes). It is assumed that the vehicle crosses the Van Allen belts at near escape velocity of 10^6 cm/sec, and approximately radially away from the earth. Under this approximation the dose D from crossing the radiation belts is

$$D\ (\text{rad}) = \bar{J} \left(\frac{d}{v}\right) \left(\frac{\overline{dE}}{dx}\right) \left(1.6 \times 10^{-8}\ \frac{\text{Rad}}{\text{MeV}}\right) \qquad (2.1)$$

where $\bar{J}$ is the particle flux in particles/(cm^2-sec), $\overline{dE}/dx$ the particle stopping power in MeV-cm^2/g for the material (silicon for COS-MOS units) under consideration, d is the radiation belt thickness in cm, and v is the vehicle velocity ($\simeq 10^6$ cm/sec). The numerical factor converts (MeV/g) to rads.

Using the models in Ref. 2.1, it is found that the proton radiation comes mostly from a shell between 1.1 Re and 2.6 Re (earth radii), which gives $d \simeq 10^9$ cm. Using $\overline{dE}/dx \simeq 15$ MeV-cm^2/g and $\bar{J} \simeq 10^4/(\text{cm}^2\text{-sec})$, gives

$$D\ (\text{protons}) \simeq 2\ \text{Rads}. \qquad (2.2)$$

For electrons, there are two regions, 1.2 Re to 1.7 Re with $\bar{J} \simeq 3 \times 10^7/(\text{cm}^2\text{-sec})$, and 3.5 Re to 6.0 Re with $\bar{J} \simeq 3 \times 10^5/(\text{cm}^2\text{-sec})$.

Using $\overline{dE}/dx \simeq 1.5$ MeV-cm^2/g (minimum ionizing), gives

$$D\ (\text{electrons}) \simeq 100\ \text{Rads}. \qquad (2.3)$$

Thus
$$D\ (\text{Van Allen Belts}) \simeq 102\ \text{Rads}. \qquad (2.4)$$

2) Solar Flare Protons - A general summary of solar flare proton intensities is given in Ref. 2.2. From Table 1-1 of Ref. 2.1, for a solar flare of average length $\bar{T}$ (sec) the maximum observed time integrated proton flux above 30 MeV is $(\bar{J}\,\bar{T})_{max} \simeq 1.4 \times 10^9$ protons/cm^2. The approximate dose from these protons is

$$D\ (\text{rads}) \simeq (\bar{J}\,\bar{T})_{max} \left(\frac{\overline{dE}}{dx}\right) \left(1.6 \times 10^{-8}\ \frac{\text{Rad}}{\text{MeV}}\right)$$

$$\simeq 300\ \text{Rads} \qquad (2.5)$$

where the stopping power for 30 MeV protons has been used. This approximate result compares well with the value of 205 rads from Ref. 2.2.

The preceding calculations show that typical doses from crossing the Van Allen belts, or from a large solar flare, are only a few hundred rads. In the course of a year, a very active sun is likely to have only a few large solar flares. Thus, in the course of a flight from earth to Mars the total estimated radiation dose is expected to be less than 10^3 rads even under very active solar conditions. Data in Ref. 2.3 suggest that 10^4 to 10^5 rads are required to produce a significant threshold shift (~1V) in COS-MOS components. Since the estimated dose is well below this dose, radiation damage is not expected to be a problem.

2.1.3 Selection of Detector

The solid state particle detector is a silicon surface barrier type. The operating voltage (to supply bias) is 25V for a 100 micron depletion depth. Since the detector leakage current can be of the order of 10μa at +50°C, the operating supply voltage has to be chosen somewhat higher to allow for the voltage drop across the filter network and load resistor. The bias supply voltage was selected at 40 volts and therefore requires a regulated DC/DC converter. Commercially available regulated converters have an inherently low efficiency at low power output levels. This problem was overcome by combining an unregulated converter of maximum 300 mw output power (Tecnetics, Incorporated) with a microcircuit regulator. Quiescent power of this combination is 180 mw and the efficiency at 40 mw output power is 20%. This compares favorably with commercial units.

In an attempt to insure a gas-tight seal for operation at low gas pressures, the original specifications for the solid state detector called for a 40 $\mu g/cm^2$ chromium layer on the front surface. Since a similar type of detector had been produced by ORTEC previously, no severe problems were anticipated. It was soon learned, however, that the specifications for a .2μa leakage current could not be guaranteed for a chromium surface detector of 300 mm^2 area. In order for the manufacturer to continue his efforts, it was necessary to relax the leakage specifications. After an extended development program ORTEC personnel found that the higher temperature required for the chromium evaporation was a severe problem. It tended to degrade the detector characteristics to a point where it was no longer useful. Smaller area detectors have been successfully fabricated, but the larger area detectors heat up too much in the center, and the surface barrier is destroyed.

In view of this setback it was decided to investigate the use of a gold-surface detector instead. It was felt that testing the gold-coated detectors through the corona region with bias applied should be a sufficient criterion for prolonged proper operation in vacuum. This test was successfully performed and is described in more detail in Appendix A. It is our judgment that if a gold-surface detector repeatedly passes the corona region test, it is completely suitable for use in this system.

2.2 System Design - Preliminary Results

The system consists of the electronics, the power supplies, a solid state detector, an α foil source which is used for the density measurements, and a calibration source. A detailed block diagram of the system is shown in Fig. 2.1.

The α source required for the gas density measurement is a 10 mCi Am^{241} foil source. An extensive discussion of the choice of this type source is given in Ref. 1.1. At a distance of about 25 cm from the source, where the detector is located, the useful α flux is of the order of $1000/cm^2$-sec. The sensitive area of the solid state detector is 3 cm^2, which results in a maximum counting rate of about 3000 cps. The small vacuum sublimed Am^{241} calibration source of .01μ Ci is deposited on a thin wire and mounted at a distance of about 1 cm from the detector surface. Its monoenergetic peak is above the highest energy of the foil source and its intensity produces a count rate of approximately 8 cps. Hence, the influence on the density dependent count rate of the foil source is negligible. The calibration source serves the purpose of verifying the overall system gain stability during flight.

The operation of the electronics is quite straightforward. Interaction of α particles from either the foil source or calibration source produce an electrical charge in the solid state detector. The charge pulses, which are proportional in magnitude to the incident particle energies, are converted to voltage pulses by the charge sensitive preamplifier (CSPA). In order to reduce pulse pile-up effects in the following voltage amplifiers the pulses are processed by the shaping amplifier to yield a 1μs rise time and a 2.5μs fall time. Overall conversion gain of the amplifiers is 2V/MeV. The voltage pulses are simultaneously coupled to two discriminators, one (LL) is set for .25 MeV and the other (UL) at 4 MeV.* When a count command from TM is received at the input of the buffer circuit, the 14 bit scaler is reset and the count gate is enabled for 2 seconds (the width of the count command pulse). During this 2-second period all pulses lying between

*The actual alpha energy required for these thresholds is 1.5 and 4.7 MeV. This limits observed alphas to region in which CO_2 and N_2 stopping power differences are small. Foil thickness over detector causes these thresholds to be higher than discriminator settings.

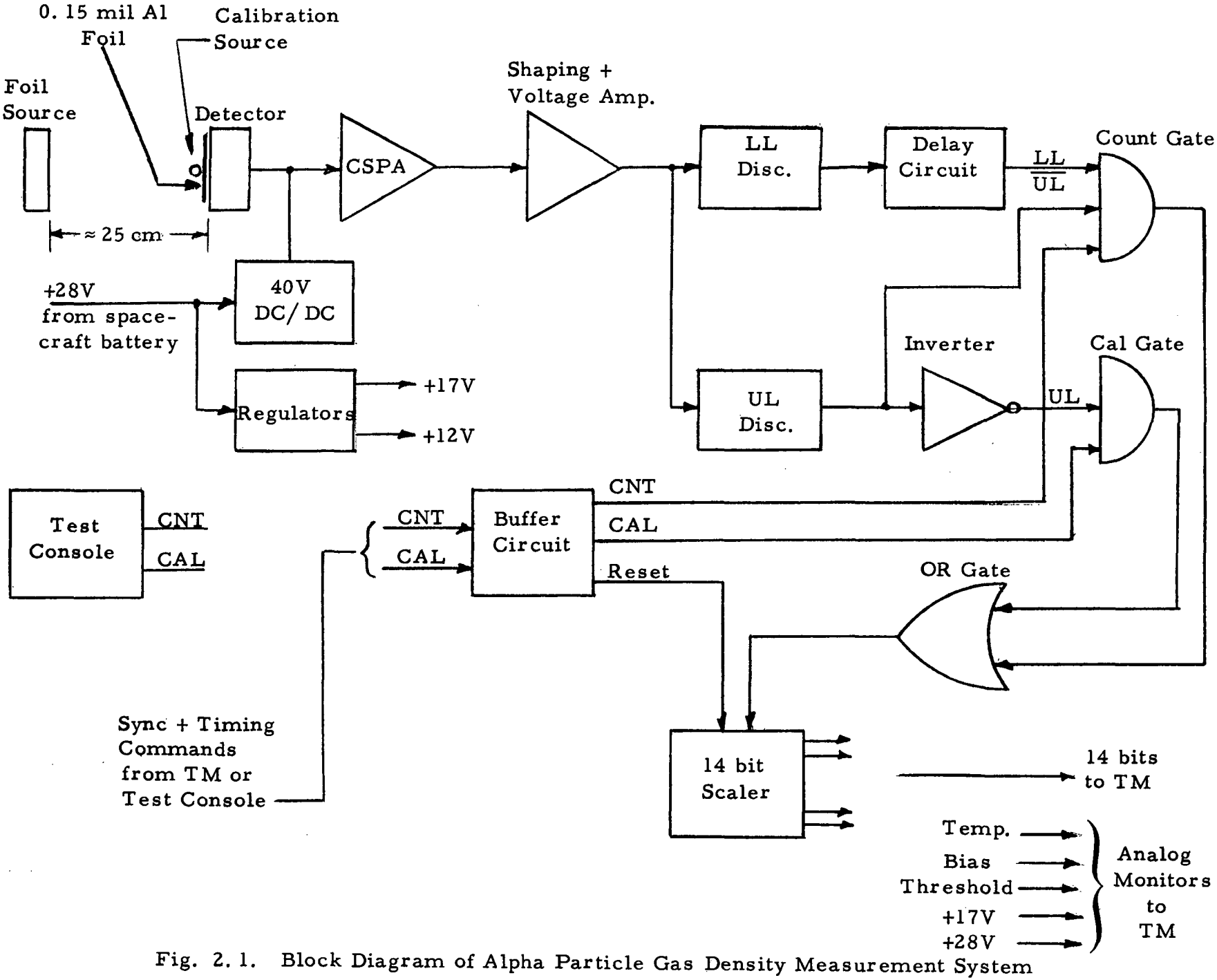

Fig. 2.1. Block Diagram of Alpha Particle Gas Density Measurement System

0.25 MeV and 4 MeV are counted, and shortly thereafter the telemetry system reads out the contents of the scaler. The calibration mode is identical in operation except that the Cal gate is enabled and only pulses above 4 MeV are counted. The sequence of Count and Cal mode of operation is determined by the main telemetry commutator. The most desirable sequence would be 10 count cycles followed by 1 cal cycle. The scaler must be read out by TM via a commutator after every count or calibration cycle. The 14 bits give a maximum of 8191 counts plus an overflow bit, a safe excess over the expected maximum of 6000.

As stated above, the Count and Cal command pulses must have a width of 2 seconds and an amplitude of 10 volts $\pm$ 1 volt. The scaler outputs are buffered and clamped to a 5 volt amplitude. Output impedance is 16 k ohms.

The power required from the spacecraft is 28V $\pm$ 4V at 320 mw. This includes the DC/DC converter for the solid state detector bias. The input power to the converter is approximately 200 mw under load. The electronics alone requires 120 mw, which is well within the design goal of 170 mw. The analog section of the electronics runs off a +17V* regulator and the digital section is powered from a +12V regulator.

In-flight monitoring of pertinent voltages and the detector temperature are provided at the output connector. The following voltages are monitored: +28V input, +17V regulator, threshold supply and the detector bias. All analog monitors are clamped at +5V, and are short circuit protected.

In order to test the feasibility and prototype models a test console was designed and constructed. It provides the 28V power to the models as well as the Count and Cal commands. The counting pulse width is switch selectable in three steps of 2, 4 and 10 seconds. The calibration pulse width is fixed at 2 seconds. Either mode is selected and manually initiated by means of a lighted push buttom. At the beginning of each Count or Cal cycle, both the console readout and the 14 bit model counter are reset. At the end of each timing pulse the content of the 14 bit densitometer counter is displayed in octal form on the console readout. The monitor voltages can be sequentially measured by means of a rotary switch connected to a single voltmeter with

*The feasibility model employed a 15V supply which was changed to 17V for better temperature stability of the amplifiers in the prototype model. Temperature errors of this supply were also reduced by use of reference diodes.

a 5V full scale deflection. The 28V input power is measured by two separate voltage and current meters. The input voltage can be continuously adjusted from 24V to 32V. A single 26 pin connector and cable carries all power and input and output signals between the model and the console.

The feasibility model was tested for temperature stability both with a pulser input and a solid state detector equivalent to that to be used for the prototype model. Over the range of -50°C to +50°C the system gain decreases by a maximum of 1.3% at both temperature extremes. The average count rate remained constant within the statistical accuracy. The leakage current at +50°C increases to about 7μa (.44μa at +25°C) with an associated increase in noise voltage of about 25%. The peak-to-peak noise is still only 20% of the lowest signal amplitude of interest and therefore poses no problem. The increase in leakage current does decrease the bias at the detector because of the voltage drop across its load resistor and the filter network. A design change was necessary to reduce this voltage drop to approximately 3.5V at +50°C.

The solid state detector (equivalent to prototype detector) was tested in vacuum from 1×10^{-4} torr through the corona region with bias applied. No degradation of resolution or increase in leakage current was observed after this test. This is a very severe test for a surface barrier detector and it can be concluded that, if it successfully passes this test, a gold-surface detector of this type will operate successfully over long periods in vacuum.

A detailed test report of the above summarized results can be found in Appendix A.

2.3 Frost Thickness Measurement

The problem of a layer of frost forming on the foil covering the solid state detector has been investigated more fully than described in Appendix D of Ref. 1.1. There it was indicated that an additional source located at a different distance could be used with an additional energy window to determine the frost layer thickness. It has been concluded that designing the present system to allow such a frost thickness measurement would make the system too complicated to be built within the specified weight, power and volume limitations.

However, the calibration mode count will give a positive indication of the presence of frost on the detector foil and, should such a layer occur,

give a warning that the gas density reading is inaccurate. This was shown by the tests described in Appendix B, where oil vapor condensed on the detector covering foil during some of the low temperature tests.

The calibration mode counts could be calibrated for a measurement of the total frost thickness on the detector foil plus the calibration source, using higher density CO_2 calibration data. This was not done for three reasons. First, since frost would form on all surfaces, including the primary source, a measurement of the frost thickness on the foil plus cal source would not be a very accurate correction to the primary density measurement, since the primary source may have a significantly different frost layer thickness than the cal source. Second, since the cal source is used mainly to check gain stability and has a low count rate, the statistical accuracy of the frost thickness measurement would be very poor. Third, from the data in Refs. 1.2 and 1.3 it appears that H_2O is a very minor constituent of the Martian atmosphere, so H_2O frost formation is not very likely, and CO_2 frost formation is likely only near the Martian poles. It is felt that the present system design with the cal count giving only a frost warning is optimum for the proposed uses of the instrument when the additional complexity and power necessary for the frost measurement are considered.

3. PROTOTYPE MODEL

3.1 Fabrication and Preliminary Tests

The electronics of the prototype model is identical to that of the feasibility model except for two changes discussed in Section 2: (1) the load resistor and filter resistor for the detector were decreased in value in order to reduce the voltage drop caused by the leakage current at elevated temperatures, and (2) the supply voltage for the analog circuits was boosted to +17 volts to achieve better temperature stability of the amplifiers.

During this phase particular attention was given to dense packaging and the selection of weight saving materials. A cordwood construction was chosen for the electronics. Two of these modules are stacked on top of each other with an electrostatic shield between them. The solid state detector is mounted in a holder adjacent to the circuit boards but electrostatically shielded from them. A bead type thermistor, with calibration as given in Fig. 3.1, is cemented directly to the detector mount. Aluminum foil of .15 mil thickness over the front of the detector prevents ambient light from reaching the detector surface.

The housing material was chosen as magnesium alloy, which gives a 50% reduction in weight compared to aluminum. The size of the total prototype model is 2-1/8 x 2-5/16 x 2-15/16 inches, or a volume of 14.4 in.^{3}. The total weight is 380 g (.85 lbs) and the power consumption including the bias converter is 320 mw at 28V. Except for size, the initial design goals were met. The volume was estimated previously to be 13 in.^{3}, slightly less than the final figure.

Prior to the density calibration measurements, discussed below, the prototype model was extensively tested in vacuum over the range from -50°C to +50°C with both foil and calibration sources. After initial difficulties with oil condensation on the detector foil at low temperatures, the cold test (0°C to -50°C) was repeated at ambient pressure. The observed gain change was less than -2% at -50°C and -1% at +50°C. The integrated counts remained stable within the statistical accuracy. Hence the prototype unit was considered suitable for gas density calibration.

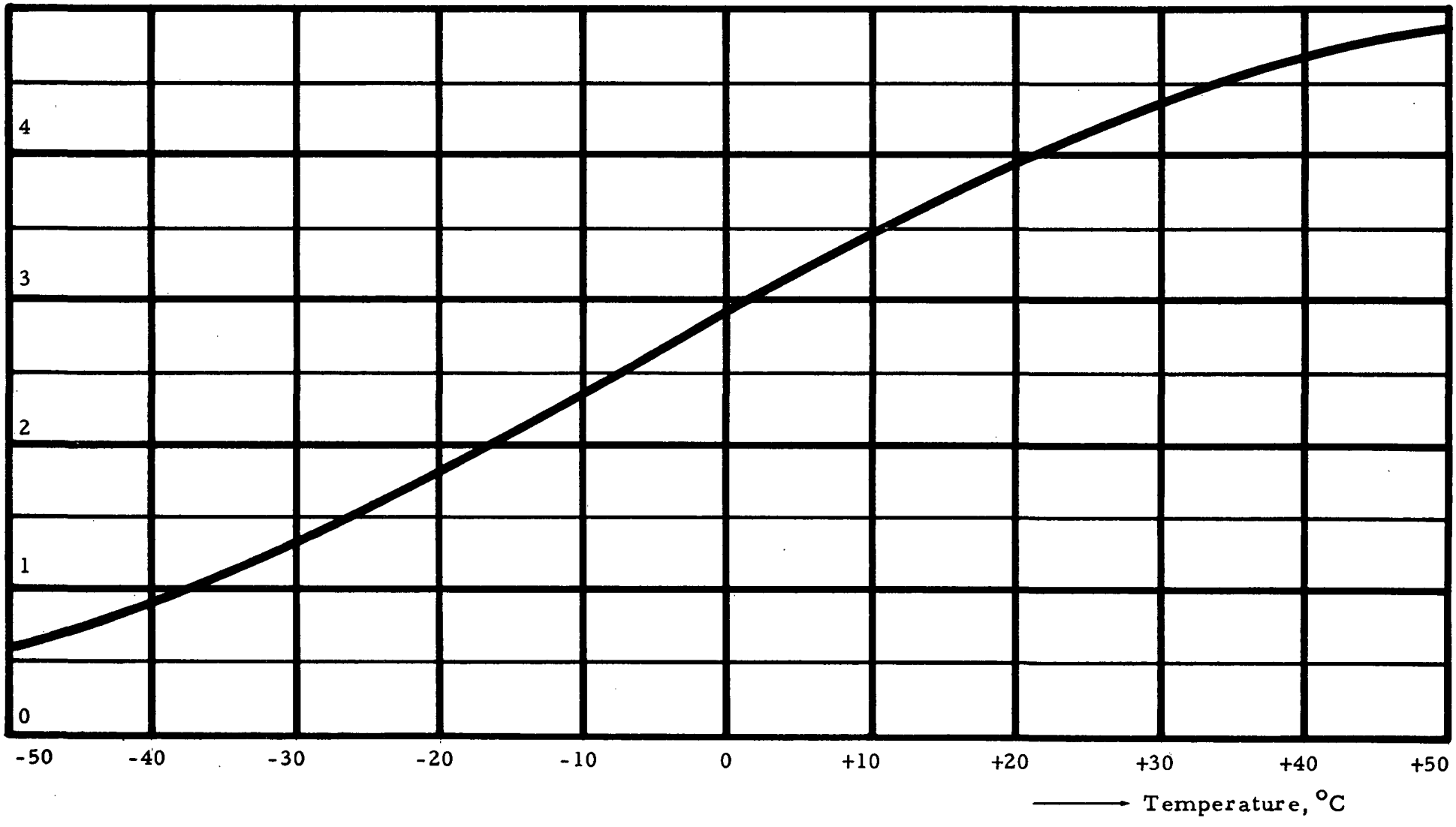

Fig. 3.1. Thermistor Calibration Curve, Volts vs. Temperature.

3.2 Density Calibration and System Accuracy

The prototype model was calibrated with Am^{241} foil source #11.68 collimated to 3/8 inch diameter circle and located 25 cm from the detector. Calibration data were taken with 100% CO_2 and 100% Ar. Since the Ar stopping power for alpha particles is about 0.67 times the CO_2 stopping power, the Ar data can be associated with an effective density ρ'_{Ar}

$$\rho'_{Ar} = \rho_{Ar} \times 0.67 \tag{3.1}$$

as described in Ref. 1.1. Since the most recent data on the composition of the atmosphere of Mars indicate a surface pressure of about 5 mb and a composition of nearly 100% CO_2 (Refs. 1.2 and 1.3), the VM-8 model referenced in Ref. 1.1 is the most appropriate (VM-2 may also be useful). These model atmospheres correspond to a surface gas density of 13.2 and 18.5 x 10^{-6} g/cm^3, respectively. The prototype was designed utilizing all the models given in Ref. 1.1, the maximum surface density being about 40 x 10^{-6} g/cm^3. A factor of two increase in the maximum useable density to 80 x 10^{-6} g/cm^3 of CO_2 was included to allow for a possible landing in a depression.

The measured calibration data are thus for an instrument designed to measure up to 80 x 10^{-6} g/cm^3 CO_2. Since Refs. 1.2 and 1.3 were published after the calibration data were taken, calibration data were not taken with the prototype for a more desirable maximum of 25 to 30 x 10^{-6} g/cm^3 CO_2. However, by shifting the source (#11.68) to 75 cm from the detector, and eliminating the 3/8" dia collimator, it would be possible to have a system design for a maximum density near 30 x 10^{-6} g/cm^3 CO_2. The calibration curve and error curves are thus shown with a second, approximate, scale of density to illustrate the expected response for this system. Since no calibration data were in fact taken with the 75 cm separation, it would, of course, be necessary to carry out this calibration with the actual source to be used for the flight.

The calibration data from two CO_2 runs are given in Table 3.1. These data are for Am^{241} source #11.68 collimated to 3/8 inch diameter, and located 25 cm from the detector (3 cm^2 area) covered by 0.15 mil of Al foil. The data from Run 1 include the calibration mode data. Table 3.2 contains the results of two calibration runs with Ar. The calibration curve based on the data of Tables 3.1 and 3.2 is shown in Fig. 3.2. The error bars shown in Fig. 3.2 are the signal count errors for a 2-second count, and the measured density errors associated with pressure gage inaccuracy. The top scale in Fig. 3.2 gives the approximate density if the full source (no collimator) is used at a 75 cm separation.

Table 3.1

Calibration Data For CO_2

Run 1			Run 2	
Density ± error (10^{-6} g/cm^3)	Signal Counts/2sec	Cal Counts/2sec	Density ± error (10^{-6} g/cm^3)	Signal Counts/2sec
0.2 ± 0.5	8253	28	0.2 ± 0.5	8237
6.4	7029	23	1.7	7935
11.1	6180	23	4.0	7514
15.9	5718	25	6.4	7000
20.6	4829	25	8.8	6306
25.4	3981	23	13.5	5277
30.1	3036	21	18.0	4488
34.8	2229	25	23.0	3662
39.6	2160	22	27.6	2960
43.8	1539	27	32.2	2403
45.7	1347	25	37.0	1843
46.7	1162	26	41.7	1398
47.4 ± 2.5	916	25	46.3	1049
54.5	604	21	46.6	1064
61.6	463	24	54.5 ± 2.5	628
66.4	190	21	66.4	159
90.1	17.3	26	90.1	22.7
113.8	2.8	22	113.8	6.0
137.5	2.2	22	137.5	2.0

Table 3.2

Calibration Data For Ar

Run 1				Run 2		
True Density	Effective density ± error $(0.67 \times \rho)$ $(10^{-6} g/cm^3)$	Signal Counts/2sec	Cal Counts/2sec	True Density	Effective density ± error $(0.67 \times \rho)$ $(10^{-6} g/cm^3)$	Signal Counts/2sec
0.2	0.1 ± 0.3	8310	18			
1.5	1.0	7750	18	1.5	1.0 ± 0.3	8117
5.8	3.9	7543	17	3.7	2.5	7821
12.3	8.2	7057	16	5.8	3.9	7550
16.6	11.1	5797	18	10.1	6.8	6916
20.9	14.0	5727	25	20.9	14.0	5333
25.2	16.9	5452	24	33.8	22.6	3854
29.5	19.7	4518	25	40.2	27.0	3203
33.8	22.6	4010	21	40.9	27.4 ± 1.7	2982
38.1	25.5	3631	23	49.5	33.1	2480
42.4	28.4	3068	23	60.2	40.3	1561
43.0	28.8 ± 1.7	3055	24	71.0	47.5	1051
49.5	33.1	2483	27	81.7	54.7	652
55.9	37.5	1954	21	92.5	61.9	345
60.2	40.3	1498	24	103.2	69.1	165
64.5	43.2	1180	25	124.7	83.5	36.5
71.0	47.5	1117	22	146.2	98.0	9.0
77.4	51.9	891	23	167.7	112.4	7.5
81.7	54.7	505	23			
86.0	57.6	528	25			
92.5	61.9	389	25			
98.9	66.3	271	21			
103.2	69.1	183	24			
107.5	72.0	125	23			
114.0	76.3	94.7	21			
120.4	80.7	79.0	25			
124.7	83.5	37.0	23			
135.5	90.8	27.3	25			
141.9	95.1	17.0	24			
146.2	98.0	11.5	24			

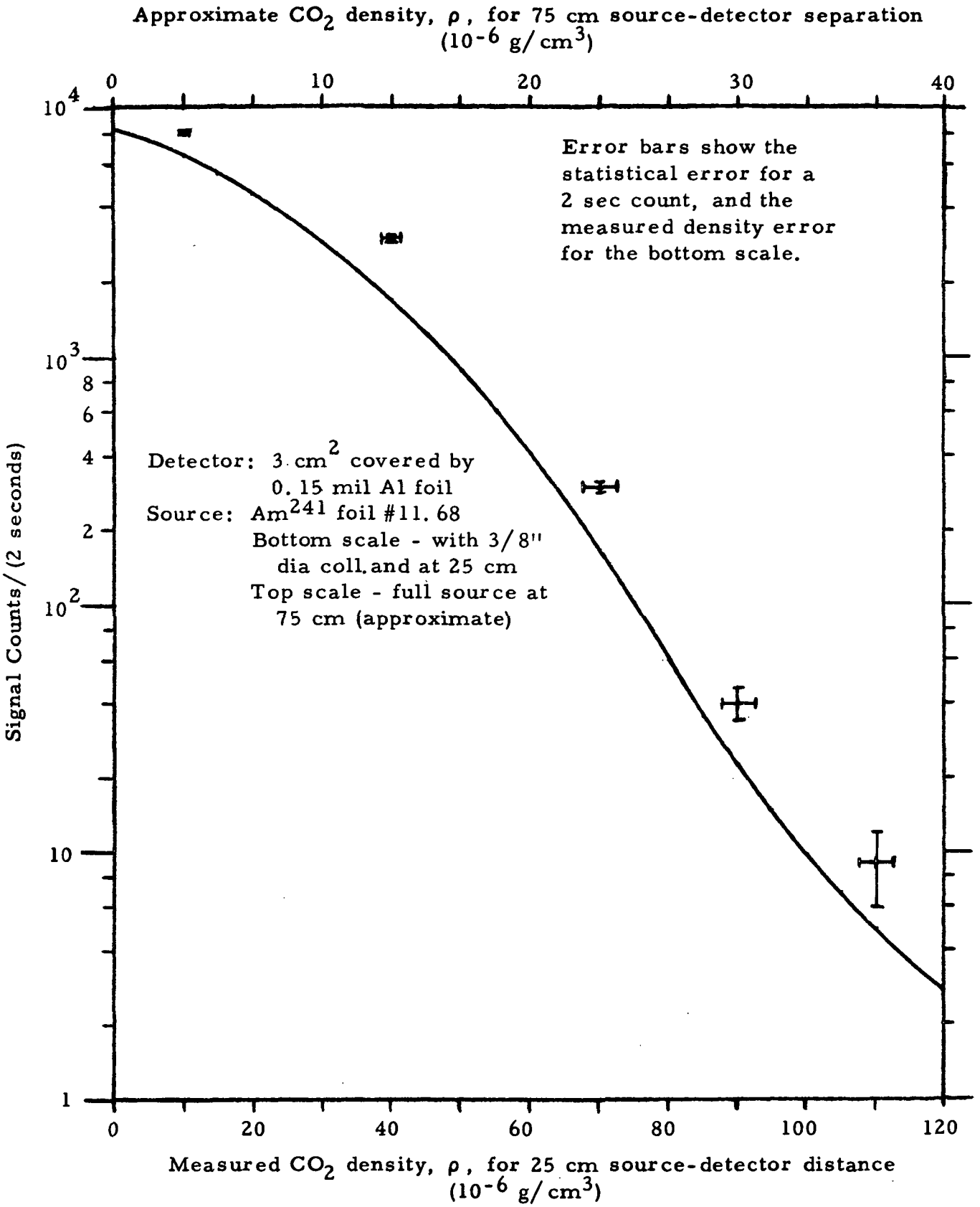

Fig. 3.2. Signal Count vs. Density Calibration Curve for CO_2.

The expected system statistical errors are shown in Fig. 3.3. The dashed curve shows the statistical density error in 10^{-6} g/cm^3, while the solid curve shows fractional density error, $\delta\rho/\rho$, in percent. The top scale again illustrates expected errors for a 75 cm source-detector separation. The solid line (fractional error) remains the same, but the dashed line (density error) must be divided by 3 to give the correct value. Again, the values for a 75 cm separation are only approximate, and are used to illustrate expected system response for a design based on the latest available Mars atmosphere data. Note that the minimum density error for the 25 cm separation is about 0.4×10^{-6} g/cm^3 CO_2, and for the 75 cm separation this becomes about 0.13×10^{-6} g/cm^3 CO_2.

The actual system used on a Mars lander may differ from either the 25 cm or 75 cm system, as it is subject to integration compromises. The configuration flown will thus have to be calibrated once it has been selected. Should a 30×10^{-6} g/cm^3 CO_2 maximum be desired, either the 75 cm separation, full source intensity configuration can be used, or else the 25 cm separation with a 0.15 mil piece of Al foil over the source can be used (this may require an increase in the collimator area to keep the maximum count rate about the same). Greater sensitivity at low densities can be obtained by covering approximately half the source area with a second piece of 0.15 mil Al foil (Ref. 1.1, pp 62 ff).

The present configuration gives about 4000 counts/sec as the maximum rate, which for a 3 cm^2 detector is about 1300/(cm^2-sec) for the alpha particle flux at the detector surface. This is slightly larger than the recommended maximum of 1000/(cm^2-sec) of Ref. 1.1, for a minimum detector lifetime of about one year. The prototype design thus has a minimum life expectancy of about 10 months under irradiation in vacuum. Reduction of the alpha flux by further collimation of the source can be used to extend the detector life, but this increases density measurement errors. Similarly, using a larger area collimator would increase the alpha flux, decrease detector lifetime, but decrease the density measurement errors. If it were possible to shield the source during transit, this latter alternative should be considered, since it provides the optimum in accuracy and/or time response.

3.3 Final Tests Summary

The final test of the unit served the purpose of checking the long term (~6 week) stability of the unit with power connected and an Am^{241} source installed. At the start, as well as at the end of the long term test, the temperature stability and the performance under vacuum were checked.

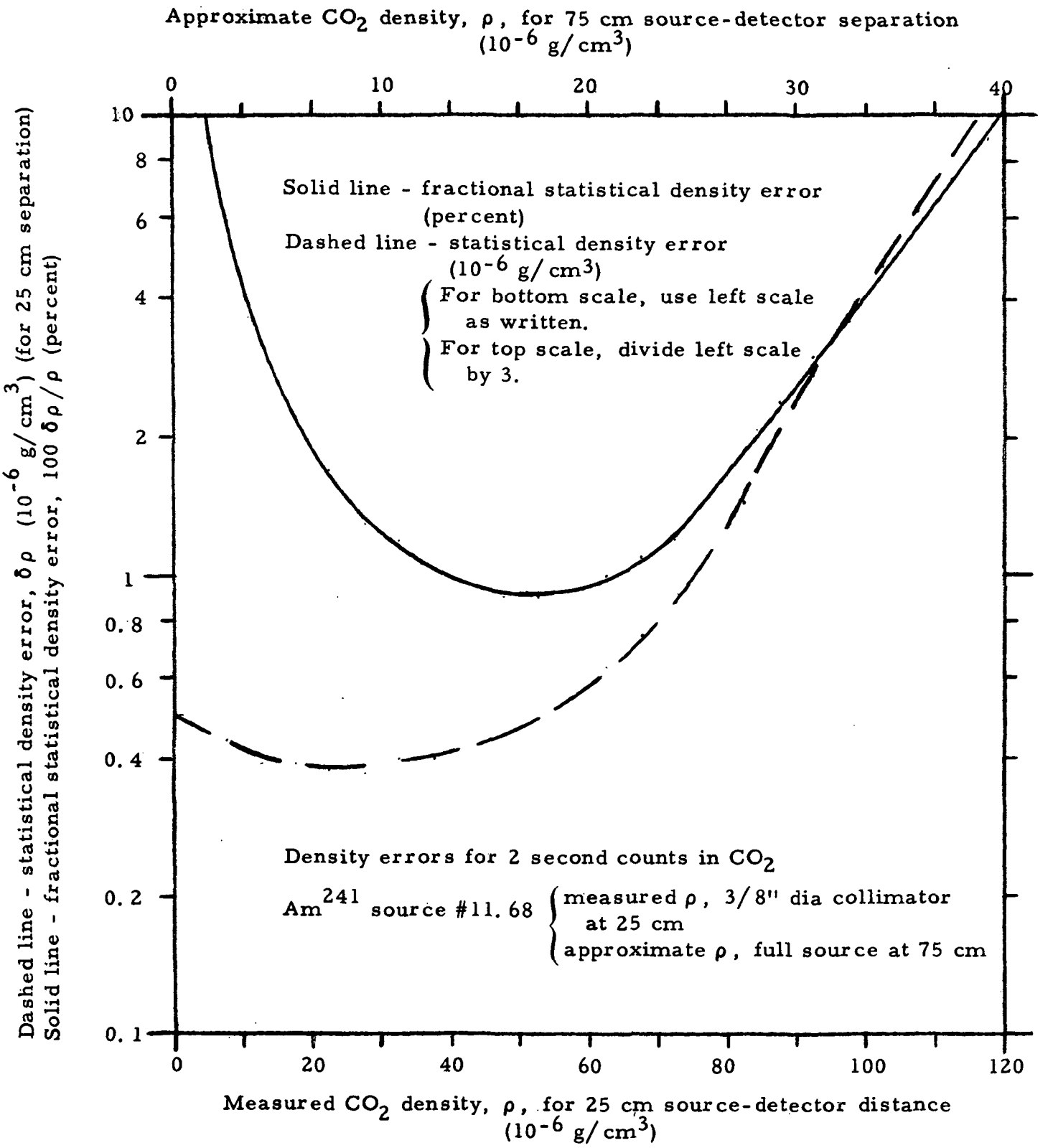

Fig. 3.3. Statistical Density Errors for CO_2 Gas Measurements. (For calibration curve in Fig. 3.2.)

No degradation either in gain or count rate was observed during the long term test. The initial and final temperature test showed the same gain shift of 1% over the range from -50°C to +50°C. No change in spectrum or gain was observed between the initial and final vacuum tests. A detailed description of the above tests is given in Appendix B of this report, and a brief summary of all tests in Appendix C.

3.4 System Specifications Summary

Photographs of the flight prototype alone and connected to the test console are shown in Figs. 3.4 and 3.5.

A brief summary of the specifications is given in Table 3.3. Statistical density accuracy for this system is given in Fig. 3.3, with the upper scale being appropriate to the most recent information regarding surface pressure (CO_2: 5 mb $\approx$ 13 x 10^{-6} g/cm^3). At high altitudes for this case:

$$\delta \rho_{stat} \approx .15 \times 10^{-6} \text{ g/cm}^3, \text{ high alt.} \qquad (3.2)$$

The only other significant error, for a system with digital-type telemetry, is that due to electronic drift. From Ref. 1.1, p. 77:

$$\delta \rho_{drift} = \frac{1.0 \times 10^{-3}}{D} \delta E_{th} \text{ g/cm}^3 \qquad (3.3)$$

where D is the source-detector separation in cm, δE_{th} is the effective variation in threshold due to electronic drift, in MeV. Taking D = 75 cm, and noting that E_{th} = 0.25 MeV, so that δE_{th} = .0025 MeV for the maximum 1% drift discussed in Section 3.3, yields:

$$\delta \rho_{drift} = 0.03 \times 10^{-6} \text{ g/cm}^3 \begin{cases} D = 75 \text{ cm} \\ \text{Elec. drift} = 1\% \end{cases} \qquad (3.4)$$

The total system error is thus less than 0.2 x 10^{-6} g/cm^3 at high altitudes in pure CO_2 for a system calibrated for a surface pressure of 5 mb. This includes a safety factor of about 2, so that the actual maximum measurable pressure is about 10 mb.

Table 3. 3

System Specifications

General Description:	Electronic system provides parallel digital counter output for all detector-amplifier pulses within, alternatively, a fixed window on external Count command or above a fixed threshold on external Cal command. Electronic thresholds are 0. 25 MeV and 4 MeV. Corresponding alpha energy thresholds are 1. 5 and 4. 7 MeV for 0. 15 mil aluminum foil over detector.
Power Input:	28V $\pm$ 4V at 11. 5 ma, 322 $\pm$ 46 mw.
Counter Output:	14 parallel bits, 4V bit level.
External Inputs:	Count command and Cal command: Pulse height 10V $\pm$ 1V, pulse width 2 seconds.
Monitor Outputs:	All analog monitors are 0 to 5V. Temperature monitor is nonlinear, and is calibrated over range -50 to +50°C; see Fig. 3. 1. Other monitors are linear, with following conversion in terms of actual unit voltage/monitor voltage:

Unit	Monitor Conversion (V/V)
Bias Supply	10. 5
Threshold Supply	1. 0
+17V	7. 3
+28V	7. 3

Density Sensor Source:	Am^{241}, 10 mCi deposited in foil.
Calibration Source:	Am^{241}, . 01 μCi evaporated on wire.
Weight:	380 g (. 85 lbs).
Size:	2-1/8 x 2-5/16 x 2-15/16 inch.
Volume:	14. 4 $in.^3$

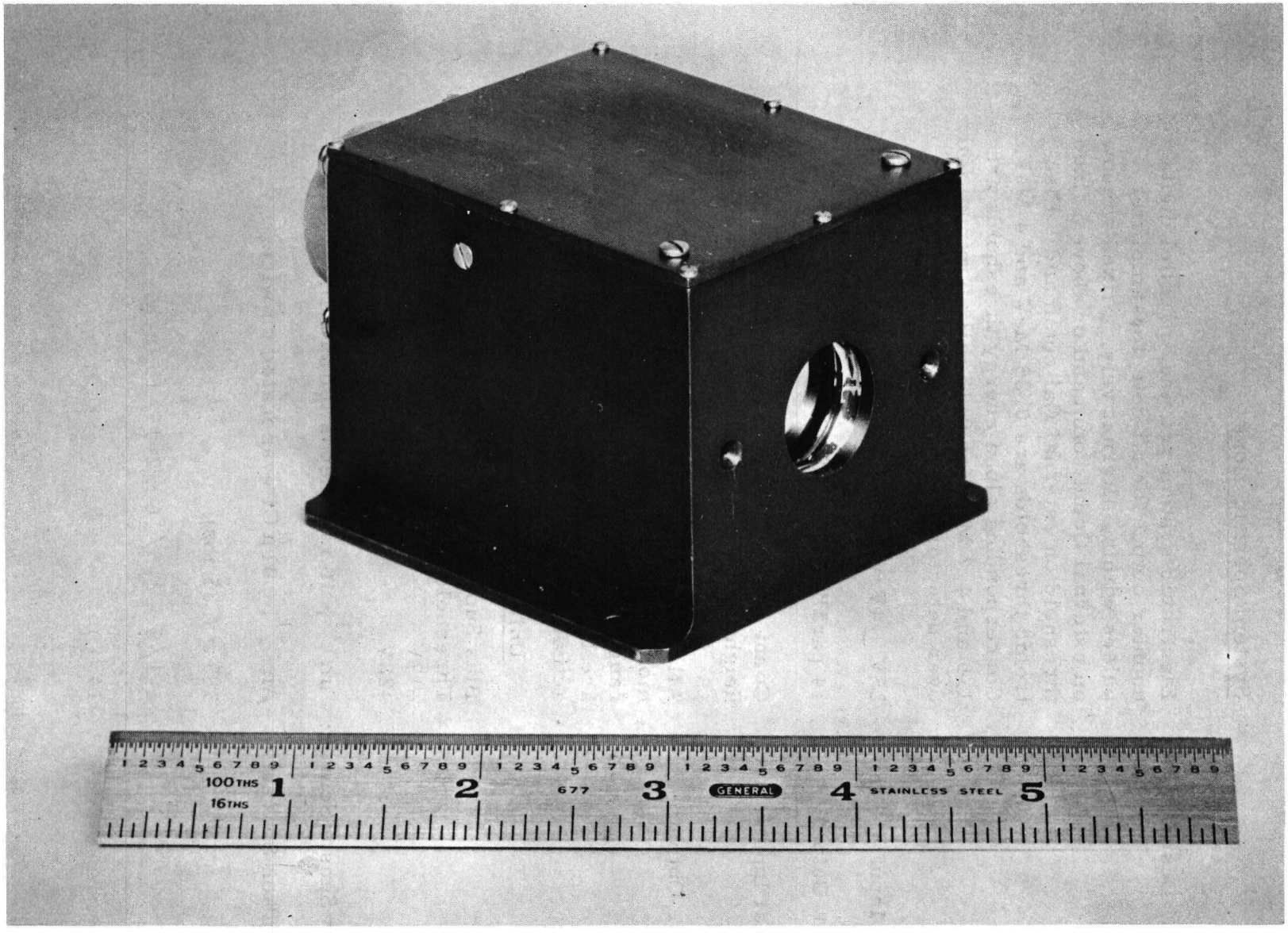

3.4 Prototype Model of Atmospheric Density Measurement System Electronics.

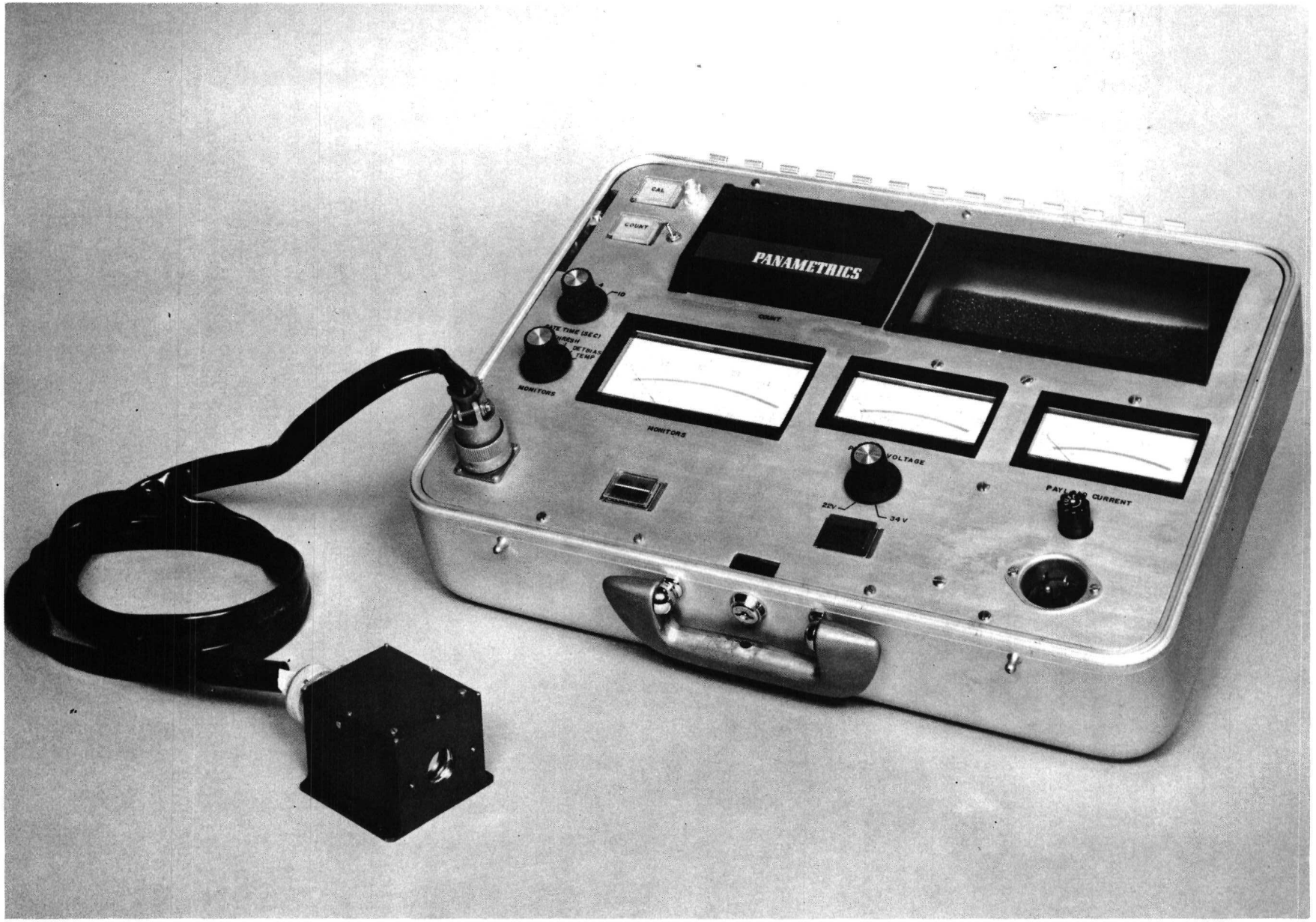

3.5 Test Console and Prototype Model.

4. CONCLUSIONS AND RECOMMENDATIONS

The principal conclusions may be summarized as follows:

1) A very low weight and power alpha particle transmission system for measurement of the atmospheric density on Martian entry has been designed, and a flight prototype has been fabricated, tested for temperature stability, and typical calibration data have been obtained. The total error at high altitudes, with 2 second time response, is less than 0.2×10^{-6} g/cm^3 for a source-detector distance appropriate to a CO_2 atmosphere with 5 mb surface pressure. Most of the error is due to nuclear statistics; very little is produced by electronic drift.

2) The system has been designed for continuous irradiation of the detector during about 10-12 months in order to allow for transit time to Mars. This places upper limits on the flux in order to assure that no significant radiation damage occur. If a shield could be placed over the source during transit, it would be possible to utilize higher fluxes during entry and hence reduce either the error or the time response.

3) Due to the high degree of electronic stability, and to the low power and weight, the system could form the fundamental basis of flight systems for applications other than measurement of atmospheric density on planetary missions, such as a planetary particle spectrometer, or a rocket-borne atmospheric density probe for the Earth's atmosphere.

As a result of the foregoing, the following recommendations are made:

1) If possible, the instrument should be flown on the mission for which it was designed.

2) Application of the instrument to other problems should be made wherever feasible. In particular, (1) in the case of rocket-borne atmospheric density probes, the more rapid time response possible where higher fluxes are tolerable should be exploited, and (2) planetary missions requiring long term stability of low power particle detection electronics should be investigated.

APPENDIX A

FEASIBILITY MODEL TESTS

A. 1 Temperature Tests with Pulser

The feasibility model was tested with a pulser input to measure the temperature stability of the electronic system. The model was placed in a controlled temperature chamber and connected to its test console and an external pulser of stable pulse amplitude. The signal from the last stage amplifier of the model was brought out with a separate coaxial cable to a multichannel analyzer (MCA). Pulse height from the amplifier was measured with the MCA and read out by means of a teletype. The pulse amplitude of the pulser was adjusted to produce an amplifier output equivalent to that of a 3 MeV α particle. Stability measurements were taken at room temperature, -50°C and +50°C each after an equilibrium time of approximately one hour. All monitor voltages and the system input current were periodically checked with the test console. The results of these tests are shown in Table A. 1.

Table A. 1

Feasibility Model, Temperature Test with Pulser

Unit/Temperature	-50°C	+25°C	+50°C
Pulser, Peak Channel	162	163	161
System input current	11. 9	11. 5	11. 5
Monitors*: Bias Supply (V)	3. 34	3. 38	3. 38
Threshold Supply (V)	4. 17	4. 18	4. 20
+15V	1. 92	2. 05	2. 10
+28V	3. 64	3. 68	3. 71
Temperature	. 58	4. 08	4. 95

****

The peak channel shifts down at both temperature extremes and is a maximum of -1. 3% at +50°C. The only monitor voltage which is outside the 1% measurement accuracy is the +15V supply monitor. As stated in Section 2. 2, this supply was redesigned for the prototype model to produce a 17V output with improved temperature stability.

*For conversions see Table 3. 3, p. 21.

A. 2 Temperature Tests with Detector

The main parameters measured during this test were the integrated counts, the detector leakage current, and the associated detector noise. The detector (equivalent to prototype detector) was mounted in the feasibility model with a . 15 mil aluminum foil over its front. A thin Am^{241} source was placed 0. 5 inches from the detector for the heat cycle. At the beginning of the cold cycle the source had to be removed temporarily to place the model inside an airtight plastic enclosure. This served the purpose of flushing the system with dry nitrogen to prevent water vapor condensation. When the source was replaced no significant effort was made to retain the same source-detector distance, which is evident from the count rate data. The leakage current was calculated from the voltage drop across the RC filter network. Because of the high count rate and 10 sec integration time an external scaler and timer had to be used. Results are given in the following table:

Table A. 2

Feasibility Model, Temperature Test with Detector

	Heat Test		Cold Test	
	25°C	+50°C	25°C	-50°C
Avg. Counts (10 s)	87481	87030	52800	52690
Leakage current at 40V bias (μa)	1. 39	7. 2	1. 40	0. 70
White Noise (mVpp)	75	100	75	75

******

The average counts remained constant within the statistical accuracy. The leakage current increased from 1. 39 μa to 7. 2 μa at +50°C without an appreciable increase in white noise. At -50°C the noise voltage remains constant which indicates that the major part of the noise spectrum can be attributed to the amplifier.

A. 3 Solid State Detector Vacuum Test

A solid state detector equivalent to that for the prototype model was tested in vacuum at about 1×10^{-4} torr. A bias voltage of 40V was applied and the front surface irradiated with a monoenergetic source of

Am^{241}. The pulse height spectrum of the detector output was measured with a multichannel analyzer. With the bias still applied, air was slowly leaked into the vacuum chamber until the pressure reached several hundred microns of mercury. The corona discharge region was passed at a pressure of several microns. The pulse height spectrum of the detector was again measured and compared with the previous one. The leakage currents were also measured before and after the corona test. The detector resolution including electronic noise remains the same and is computed to be 56 keV which is within specifications. The leakage current measured 1.4 μa and showed no change after the corona test. The test result shows that the increased gold layer on the front surface is sufficient to make the detector gastight. This prevents electrical breakdown of the barrier layer when subjected to pressures in the corona region.

As a result of these tests it was concluded that this type detector from ORTEC will perform satisfactorily in the prototype model over prolonged periods in vacuum.

APPENDIX B

PROTOTYPE MODEL TESTS

B. 1 Vacuum-Temperature Test

The prototype with the same detector used for the feasibility model was mounted inside an aluminum block of approximately 5 in. diameter and 6 in. length. A copper pipe was coiled around the outside of the block, which served to cool the unit by flowing CO_2 through the pipe. The coil then was wrapped with a heating blanket.

To determine the gain stability of the prototype system, an Am^{241} calibration source was mounted directly in front of the solid state detector. The source consists of .020 in. diameter, platinum wire with Am^{241} vacuum sublimed on the surface. A foil source of Am^{241} was placed at a distance of 10 in. from the detector. The foil source emits a continuous spectrum of α particles and serves to determine the system' s counting rate versus gas density. During the temperature test however, the pressure in the vacuum chamber was kept below 100 microns which is outside the density range capability of the system. This procedure assured that the stability measurements were not affected by changes in gas density. At low gas pressure, therefore, the foil source was used to check overall system stability by observing the system' s counting rate.

With the aluminum block assembly inside the vacuum chamber, the prototype was connected to its external test console through a vacuum connector. The test console provides the 28V power to the prototype and monitors various bias voltages, the temperature and the digital counter output of the prototype. The output of the last stage pulse amplifier was brought out through a temporary coax to a multichannel analyzer.* Temperature of the aluminum block was monitored by a calibrated thermistor, attached to the surface.

During the first cold cycle an excessive gain shift was observed which was not in line with previous cold cycle results at ambient pressure. Inspection of the unit revealed that a film of pump oil had condensed on the foil which covers the detector. To overcome this problem the low temperature test from 0°C to -50°C was repeated at ambient pressure. The gain change relative to that at 0°C is less than -2% at -50°C and -1%

*The output of this amplifier is marked on the circuit board with a red dot.

at +50°C. The counts integrated over a period of 10 seconds remained stable within the statistical accuracy.

B. 2 Final Tests

The main purpose of the final tests was to determine long term effects on the detector and electronics with the power on and a Am^{241} thin source irradiating the detector continuously. At the beginning and at the conclusion of the long term stability test a temperature test at ambient pressure and a vacuum test were performed.

As in all previous measurements, the test console furnished the power and served to read out the 14 bit scaler. An auxiliary output from pin 5* of the voltage amplifier was brought out with a coaxial cable. This output was connected to a multichannel analyzer in order to record the pulse height spectrum of the solid state detector. This detector is the second purchased from ORTEC with specifications equivalent to the feasibility detector. The counts were integrated over a 2-second period with a Cal command from the test console. Special attention was given to the periodic calibration of the multichannel analyzer with a mercury pulser.

The pulse height spectrum taken during the vacuum test showed a normal resolution with no deterioration and no gain change after the long term test. The results of the initial temperature test were much improved over those stated in Section B. 1. The gain shift relative to that at room temperature is -1% at -50°C and 0% at +50°C. The average 2-second count is 625 and remains constant, within statistical accuracy, over the entire temperature range. The final temperature check showed essentially the same results. The fact that the measured temperature stability of the gain is improved, compared to earlier results with this model, is attributed principally to the fact that the MCA was periodically calibrated with a mercury pulser. Results are given in Table B. 1.

Photographs of the CRT display of the multichannel analyzer (Figs. B. 1 and B. 2) show the energy spectra of an Am^{241} source before and after the long term tests, respectively. The spectra were taken in vacuum with a . 15 mil aluminum foil over the front of the solid state detector. The spectrum peak before and after 42 days of operation appears in channel 78 of the MCA, and clearly shows a stable gain behavior of the prototype amplifiers. The spectra were taken for slightly different

*Location of this pin in the model is marked with a red dot.

times and source location, so the statistics are not identical. Neither the system resolution or gain appear to have changed measurably during the stability test.

The photographs of Figs. B. 3 and B. 4 were obtained from the MCA display during the initial temperature tests. These tests were performed at ambient pressure, with a source-detector spacing of about 1/32 of an inch. The spectrum obtained at +25°C is shown in Fig. B. 3 and that at +50°C is shown in Fig. B. 4. Both spectra peak in channel 87 of the MCA and prove that no gain shift has occurred over this temperature range. The spectrum taken during the cold test (-50°C) looks much the same as that taken at +50°C except that its peak has shifted by one channel to channel 86. This represents a gain change of about -1%. Spectra taken during the temperature test made after the long term stability test were also similar, as suggested by the data of Figs. B. 1 and B. 2.

The results of the above tests demonstrate that the gain was stable to 1% over the range ± 50°C during the 42 day stability test. Nonoperational sterilizability tests at higher temperature were not carried out, principally because exact specifications for the tests were not available. Specifications for the system components, however, suggest that no difficulty would be experienced in nonoperational temperature cycling up to at least 150°C.

Table B. 1

Prototype Model, Final Temperature Test

Monitor*/Temperature	-50°C	+25°C	+50°C
Bias Supply (V)	3. 44	3. 48	3. 48
Threshold Supply (V)	4. 60	4. 60	4. 61
+17V (labeled +15V)	2. 31	2. 33	2. 33
+28V	3. 73	3. 75	3. 75
Temperature	. 60	4. 15	4. 88

*For conversions see Table 3. 3, p. 21.

****

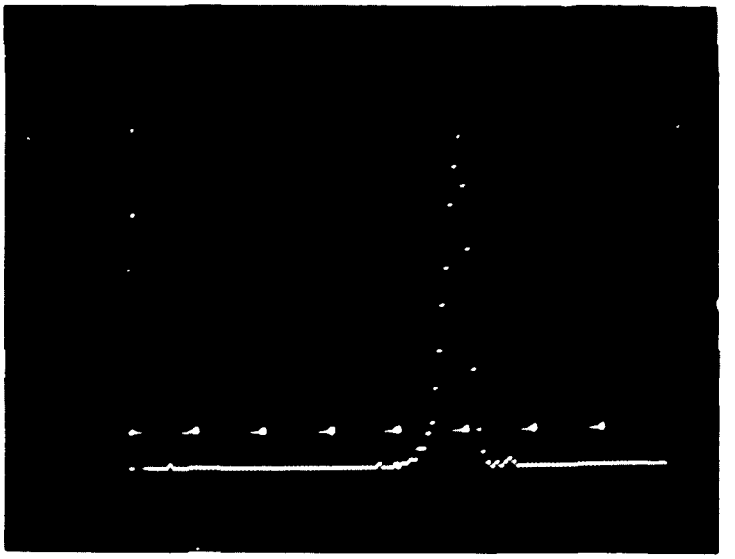

Fig. B. 1. Energy Spectrum of Am^{241}, obtained from Prototype Model before long term test.

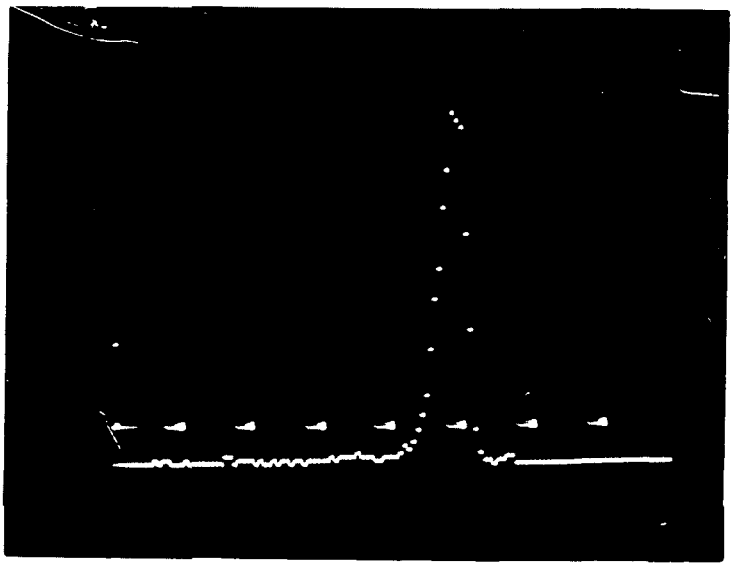

Fig. B. 2. Energy Spectrum of Am^{241}, obtained from Prototype Model after 42-day long term test.

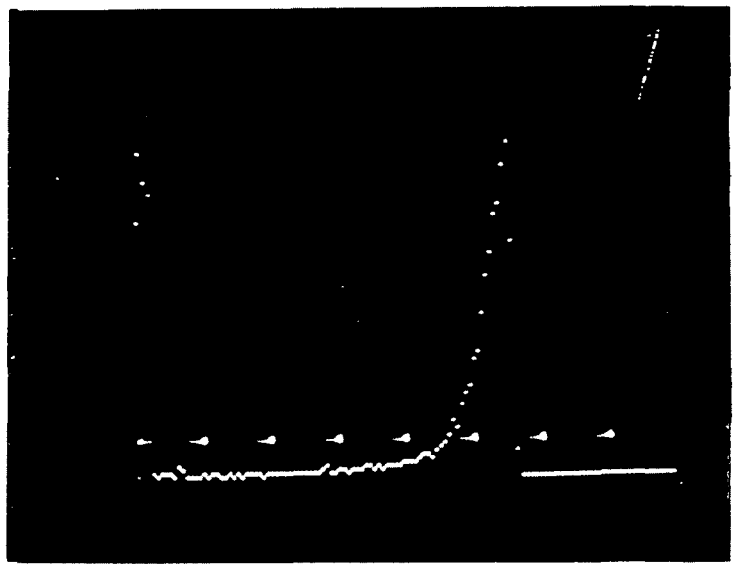

Fig. B. 3. Energy Spectrum of Am^{241}, obtained from Prototype Model at +25°C.

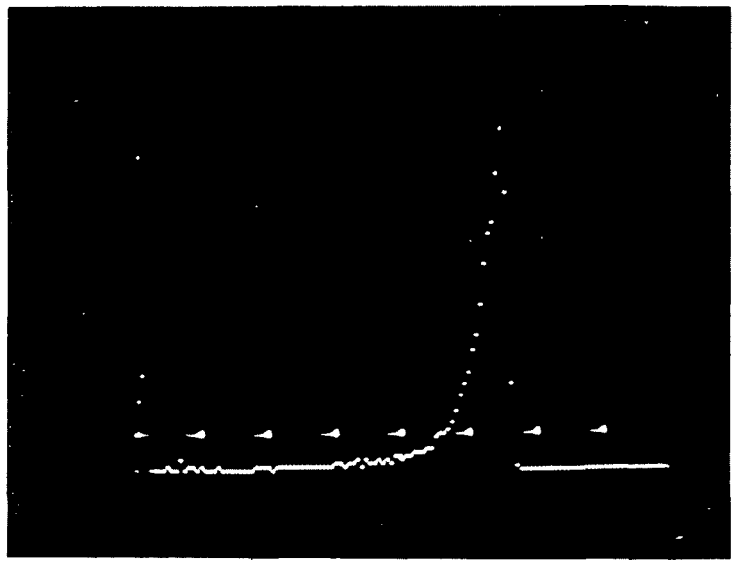

Fig. B. 4. Energy Spectrum of Am^{241}, obtained from Prototype Model at +50°C.

APPENDIX C

TABULAR TEST SUMMARY

For convenience the following table contains a short summary of the feasibility and prototype model tests, along with the general section reference, test conditions and principal conclusions.

Table C. 1

Brief Summary of All Tests

Test/Objective	Section Ref.	Conditions and Principal Results
Feasibility Model		
Temp. Test with Pulser/ Gain Stability	A. 1	Temp. varied $\pm$ 50°C. Maximum gain shift -1. 3% at -50°C. Only significant voltage change was in 15 volt supply.
Temp. Test with Detector/ Count Stability and Detector Noise	A. 2	Temp. varied $\pm$ 50°C. No significant change in count or appreciable increase in noise.
Detector-Vacuum Test/ System Vacuum Performance	A. 3	Pressure decreased through corona region. No change in detector characteristics or any systems difficulties.
Prototype Model		
Vacuum-Temperature Test/Gain Stability Under Vacuum	B. 1	Temp. varied under vacuum $\pm$ 50°C. At -50°C excessive gain shift was observed due to condensation of oil on detector foil.
Temp. Test/Gain Stability	B. 1	Temp. varied $\pm$ 50°C. Maximum observed gain shift -2% at -50°C.
Long Term Test/Gain and Count Stability	B. 2	Detector irradiated for 42 days at fixed rate. No measurable gain or count shift.
Final Temp. Test/Gain and Count Stability	B. 2	Temp. varied $\pm$ 50°C before and after long term test. Maximum observed gain shift -1% at -50°C. No significant change in count.

****

REFERENCES

1.1 F. A. Hanser and B. Sellers, Feasibility Study of Alpha Particle Densitometers for Measuring Planetary Atmospheric Density, Final Report, Contract No. NAS1-8487, NASA CR-66825 (1969).

1.2 M. B. McElroy, Mars, an Evolving Atmosphere, Science, pp. 443-445 (28 Jan. 1972).

1.3 A. P. Ingersoll and C. B. Leovy, The Atmosphere of Mars and Venus, Ann. Rev. Astr. and Astrophys. 9, 147 (1971).

2.1 Models of the Trapped Radiation Environment, NASA SP-3024, in 4 volumes:

J. I. Vette, Volume I: Inner Zone Protons and Electrons (1966).

J. I. Vette, A. B. Lucero, and J. A. Wright, Volume II: Inner and Outer Zone Electrons (1966).

J. I. Vette, A. B. Lucero, and J. A. Wright, Volume III: Electrons at Synchronous Altitudes (1967).

J. H. King, Volume IV: Low Energy Protons (1967).

2.2 H. H. Malitson, and W. R. Webber, A Summary of Solar Cosmic Ray Events, in F. B. McDonald, ed., Solar Proton Manual, NASA TR R-169 (1963).

2.3 W. Poch and A. G. Holmes-Siedle, Permanent Radiation Effects in Complementary-Symmetry MOS Integrated Circuits, IEEE Trans. Nucl. Sci., NS-16, #6, p. 227 (Dec. 1969).